INTERNATIONAL JOURNAL OF PRECISION ENGINEERING AND MANUFACTURING Vol. 17, No. 10, pp. 1351-1358 OCTOBER 2016 / 1351
DOI: 10.1007/s12541-016-0160-3 ISSN 2234-7593 (Print) / ISSN 2005-4602 (Online)

Research on the Design of the Ultra-High-Precision Positioning Control Error Compensation

Dae-Kwang Park[1], Gyung-Il Lee[2], Jia-Chen Gao[2], and Jae-Yeol Kim[3,#]

1 Department of Advanced Parts and Materials, Graduate School, Chosun University, 309, Pilmun-daero, Dong-gu, Gwangju, 61452, South Korea
2 Department of Mechanical System Engineering, Graduate School, Chosun University, 309, Pilmun-daero, Dong-gu, Gwangju, 61452, South Korea
3 Department of Mechanical System Engineering, Chosun University, 309, Pilmun-daero, Dong-gu, Gwangju, 61452, South Korea
Corresponding Author / E-mail: jykim@chosun.ac.kr, TEL: +82-62-230-7745, FAX: +82-62-230-7035

KEYWORDS: Ultra-high-precision positioning, Error compensation tool servo, Pitching error, Rolling error, Yawing error

Active researches on milli-structures and micro-machines have been conducted in advanced countries, and micro-machining technology is one of the core items of the researches. The current technical backgrounds of micro-machining can be divided into semiconductor-based machining, such as lithography and etching, and conventional mechanical machining such as cutting, grinding, and electro-spark machining. The former can be limited due to their materials or thickness, and the latter, while having good productivity, suffer from a less-than superior finishing surface. Therefore, the cutting work could be reasonable in terms of superior productivity and a greater degree of freedom. Conventional ultra-high-precision cutting technology can be used for surface machining, but it has not yet been used to produce ultra-fine components. Therefore, researches on the preparation of ultra-high-precision micro-components in three-dimensional spaces with the milling technique using a single crystal diamond bite are underway. In this study, finite element analysis (FEA) was used to determine the safety and control performance of the micro-stage for the design of an elastic-hinge-type stage using a piezo-electric element.

Manuscript received: July 5, 2015 / Revised: July 28, 2016 / Accepted: July 29, 2016

NOMENCLATURE

Fm = main cutting force
Fr = radial/thrust cutting force
Fa = feed cutting force
N = shape function
$\hat{a}$ = parameter
B = deformation rate matrix
E = Young's modulus
v = Poisson ratio
σ_{ij} = stress
ε_{ij} = deformation rate
f^e = applied force
K^e = element rigidity matrix
a^e = knot parameter

1. Introduction

Milli-structures and micro-machines have been studied actively in many advanced countries, and micro-machining is one of the key research topics that are growing in importance. Current micro-machining technologies are divided into two groups: those derived from semiconductor manufacturing such as lithography and etching, and those from general machining technology such as milling, polishing, and electro-spark machining.

The application of the former can be limited, however, depending on its material thickness or property, whereas the latter, despite its high productivity, still poses difficulty in achieving a high-quality polished surface. It is therefore desirable to adopt a machining technology with high productivity and versatility. Conventional ultra-high machining technology allows the operator to achieve the desired level of polished surface, but such technology has never been truly tested over time in the machining of ultra-high-precision parts using a lathe. Accordingly, researches are underway to enable the manufacture of ultra-high-precision three-dimensional components with a milling machine equipped with a single crystal diamond cutting tool.[1-4]

Ultra-high-precision positioning, the key technology in implementing such a nano-level manufacturing process, is realized by tapping into a suite of integrated technologies that span such varied areas as mechanics, electronics, optics, control engineering, design, and machining. Scanning tunneling microscopy (STM) and atomic force microscopy (AFM), ultra-high-precision positioning technologies used currently in physics, for example, allow researchers to perform single-atom-level measurement or manipulation to barely up to a few micro-meters. Industries demand, however, an ultra-high-precision positioning technology that is capable of a few-hundred-mm's stroke while maintaining nano-meter precision in the areas of ultra-micro-machining, ultra-high-precision measurement, semiconductor wafers, optical communication parts, and photo magnetic memories, spurred largely by the trends of the ever-rising density and size of components, which makes the securing of generic technologies that will support such demand an urgent agenda item among researchers.[5-11]

To meet such industry demand, the authors reviewed and analyzed the stability and control performance of a structure through a finite element analysis of the compensation for the yawing error, rolling error, and pitching error before assembling the Ultra-high-precision Cutting Unit 3 (UP3), which is necessary for the structural design and ultra-high-precision machining of the Error Compensation Tool Servo (ECTS) in the micro-stage section.

2. ECTS Design

2.1 Configuration of the Micro-stage

The micro-stage used in the ultra-high-precision positioning system usually adopts piezo-electric elements, which are classified into the inchworm type, the friction drive type, and the flexure hinge type. While the friction drive type boasts of an extended moving distance due to the shearing strain or the tube structure of the piezo-electric elements, it is difficult to model its non-linearity while it is in operation. The inchworm type can easily achieve an extended moving distance due to the laminated structure of the piezo-electric element along its length, but this complicates the design of the control system.

Though the flexure hinge type that was selected for this study has limited applications and is fragile, it is capable of linear feeding movement and is fast-responding and frictionless, thus demonstrating excellent wear resistance. It is also excellent compared to other types in terms of safety, controllability, and precision.

The flexure hinge type that was adopted for the micro-stage has a symmetrical structure and is flexible along the length of the feeding movement but rigid along other directions. As the hinge moves along the direction of the movement in the flexure hinge type, the design of the hinge is the key factor that governs the property of the micro-stage.

When designing a flexure hinge, special consideration must be given for its rigidity, with the formula proposed by Paros and Weisbord being frequently used in designing the hinge. This theory is mathematically explained in Eq. (1) and Fig. 1.[12-14]

$$K_s = \frac{E_p^{\frac{7}{2}}}{20R^{\frac{1}{2}}} \text{ (When there is a rectangular notch)} \quad (1)$$

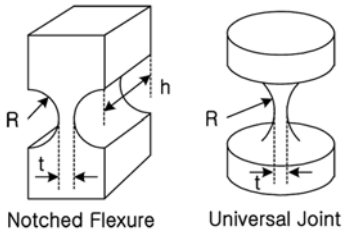

Fig. 1 Flexure hinge of Ultra Precision Stage

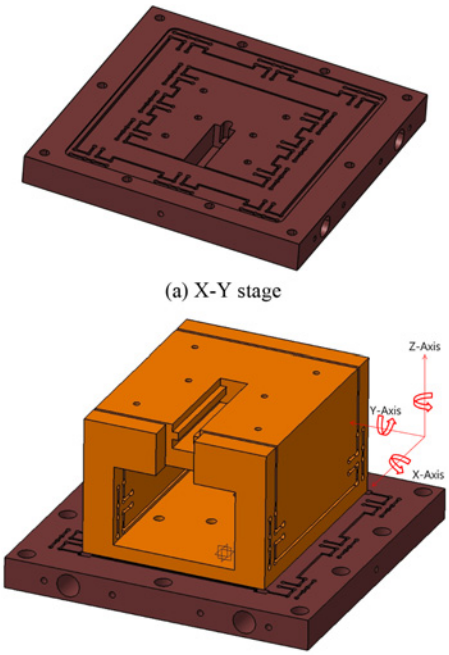

(a) X-Y stage

(b) X-Y stage and Z stage

Fig. 2 Modeling of the ultra-high-precision stage

The flexure hinge designed for this experiment was easily cut with a wire and adopted aluminum to minimize the thermal strain. Its micro-movement stage had a displacement of ±20 μm and a practical displacement of ±5 μm. The micro-stage is a symmetrical structure that is directly connected to the piezo-electric driver. The rigidity of the stage was analyzed by applying the force during the machining and force displacement of the piezo-electric element. Finite element analysis was used to minimize trial and error in the development of the ultra-high-precision positioning system.[15]

3. Interpretation of ECTS

3.1 Interpretation of the finite elements

The Error Compensation Tool Servo (ECTS) was designed to respond to pitching, rolling, and yawing errors, which are detected during material machining along the lengths of the X, Y, and Z axes, respectively. The micro-stage is directly connected to the piezo-electric actuator, and ECTS is designed to maintain the initial rigidity through the reverse-interpreting artificial machining force (Fm: main cutting

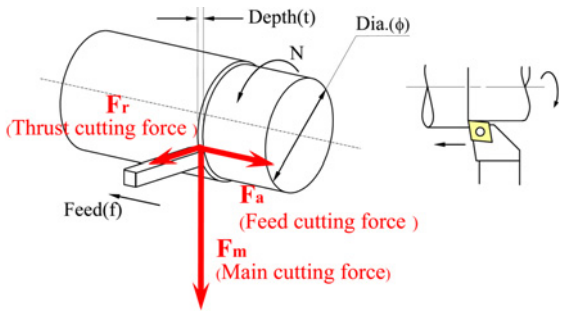

Fig. 3 Cutting force of the ultra-high-precision cutting unit

force; Fr: radial/thrust cutting force; and Fa: feed cutting force) of UP3. Its rigidity must be higher than the maximum machining force, as the displacement during the machining, which happens when the operator concentrates only on the control performance, makes it difficult to achieve optimal control performance. Fig. 3 shows the cutting force when the feed value is 0.3 mm/rev and the speed of the main axis is 150 m/min.

With the finite element analysis, the researchers intended to figure out if the displacement of the piezo-electric element can be controlled and to identify the stability and property per compensation for the rolling, yawing, and pitching errors detected during the machining. The 3D Solid Element method was adopted for the finite element analysis, and its material property was assumed to have been elastic. The force from the piezo-electric element was considered focused on a single point. The preceding conditions are mathematically expressed as follows.

$$\hat{\varepsilon}=\begin{bmatrix}\varepsilon_{xx}\\ \varepsilon_{yy}\\ \varepsilon_{zz}\\ \varepsilon_{xy}\\ \varepsilon_{yz}\\ \varepsilon_{zx}\end{bmatrix}=\begin{bmatrix}\partial u/\partial x\\ \partial v/\partial y\\ \partial w/\partial z\\ \partial v/\partial z+\partial w/\partial y\\ \partial w/\partial x+\partial u/\partial z\\ \partial u/\partial y+\partial v/\partial x\end{bmatrix} \tag{2}$$

$$\hat{\varepsilon}=\frac{1}{2}\begin{bmatrix}\psi_x^T & 0 & 0\\ 0 & \psi_y^T & 0\\ 0 & 0 & \psi_z^T\\ 0 & \psi_z^T & \psi_y^T\\ \psi_z^T & 0 & \psi_x^T\\ \psi_y^T & \psi_x^T & 0\end{bmatrix}(\psi_x\psi_y\psi_z)=\frac{1}{2}\hat{A}\hat{\psi} \tag{3}$$

$$\psi_x^T=\begin{bmatrix}\frac{\partial_u}{\partial_x} & \frac{\partial_v}{\partial_x} & \frac{\partial_w}{\partial_x}\end{bmatrix},\quad \psi_y^T=\begin{bmatrix}\frac{\partial_u}{\partial_y} & \frac{\partial_v}{\partial_y} & \frac{\partial_w}{\partial_y}\end{bmatrix},\quad \psi_z^T=\begin{bmatrix}\frac{\partial_u}{\partial_z} & \frac{\partial_v}{\partial_z} & \frac{\partial_w}{\partial_z}\end{bmatrix} \tag{4}$$
$$\hat{de}=\frac{1}{2}d(\hat{A}\hat{\psi})=\frac{1}{2}d\hat{A}\hat{\psi}+\frac{1}{2}d\hat{A}d\hat{\psi}=\hat{A}d\hat{\psi}$$

The displacement $\hat{\psi}$ using the shape function N and the knot parameter $\hat{a}$ is mathematically explained as $\hat{\psi}=\hat{G}\hat{a}$ and $d\hat{\varepsilon}=\hat{A}\hat{G}d\hat{a}$, and its deformation rate matrix B is expressed as follows.

$$B=\hat{A}\hat{G} \tag{5}$$

$$\hat{G}=\begin{bmatrix}\frac{\partial N_1}{\partial x} & \frac{\partial N_2}{\partial x} & \cdots\\ \frac{\partial N_1}{\partial y} & \frac{\partial N_2}{\partial y} & \cdots\\ \frac{\partial N_1}{\partial z} & \frac{\partial N_2}{\partial z} & \cdots\end{bmatrix} \tag{6}$$

E and v are Young's modulus and the Poisson ratio, respectively, and their matrix D per material is as follows.

$$D=\frac{E(1-v)}{(1+v)(1-2v)}=\begin{bmatrix}1 & \frac{v}{(1-v)} & \frac{v}{(1-v)} & 0 & 0 & 0\\ \frac{v}{(1-v)} & 1 & \frac{v}{(1-v)} & 0 & 0 & 0\\ \frac{v}{(1-v)} & \frac{v}{(1-v)} & 1 & 0 & 0 & 0\\ 0 & 0 & 0 & \frac{(1-2v)}{2(1-v)} & 0 & 0\\ 0 & 0 & 0 & 0 & \frac{(1-2v)}{2(1-v)} & 0\\ 0 & 0 & 0 & 0 & 0 & \frac{(1-2v)}{2(1-v)}\end{bmatrix} \tag{7}$$

Accordingly, the relationship between the stress σ_{ij} and the deformation rate ε_{ij} can be expressed as follows.

$$\bar{\sigma}=\begin{bmatrix}\sigma_{xx}\\ \sigma_{yy}\\ \sigma_{zz}\\ \sigma_{xy}\\ \sigma_{yz}\\ \sigma_{zx}\end{bmatrix}=D\bar{\varepsilon} \tag{8}$$

$$K^e=\int_{v^e}B^TDBdv^e \tag{9}$$

In conclusion, the Finite Element Formation for a certain 3D element is calculated using the following formula:

$$f^e=K^ea^e \tag{10}$$

wherein f^e is the applied force, K^e is the element rigidity matrix and a^e is the knot parameter.

3.2 ECTS finite element modeling

Nastran FX2010, a popular commercial finite element analysis program that is widely used in industry, was employed for the conduct of a finite element analysis in this study. The structure model was simplified as shown in Fig. 4 for accurate mesh work, and a separate model was made on the flexure hinge for accurate structural analysis, with their respective contact areas combined using a weld contact.

3.2.1 Static analysis considering the machining force

For accurate finite element analysis of the flexure hinge, a 3D element mesh was created from a 2D mesh by relying on element mesh extraction, and a 3D Auto mesh was applied to the rest of the structure. Regarding the boundary conditions for ECTS, fixed restraint was applied to the outer area of the X-Y stage, and a 150 N main cutting force, 100 N feed cutting force, and 50 N thrust cutting force were

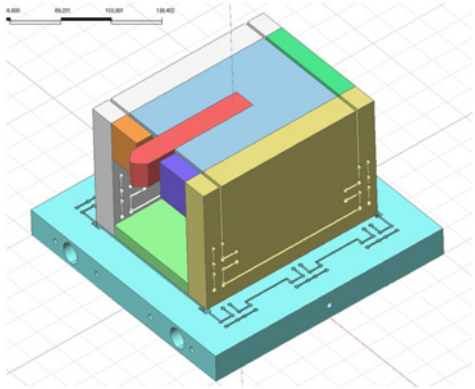

(a) Separate model structure

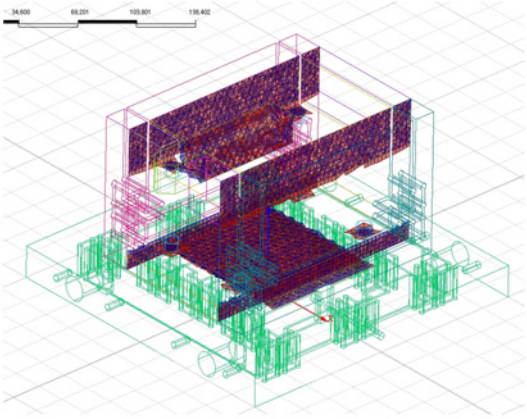

(b) ECTS of the welded structures

Fig. 4 Finite element analysis model

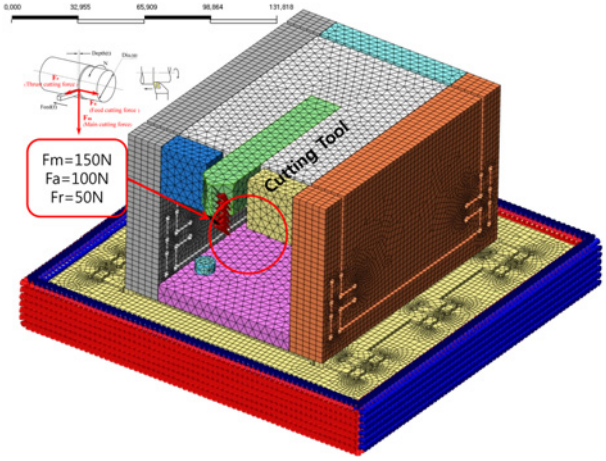

Fig. 5 FEM model of ECTS (Error Compensation Tool Servo)

Table 1 Structure and specifications of the ECTS machine

Material	Young's modulus (N/mm^2)	Poisson's ratio	Mass density (kg/mm^3)	Tensile stress (N/mm^2)
ECTS (aluminum)	71,800	0.336	2.86×10^{-6}	482.5
Cutting tool (tungsten)	400,000	0.28	2.86×10^{-6}	980

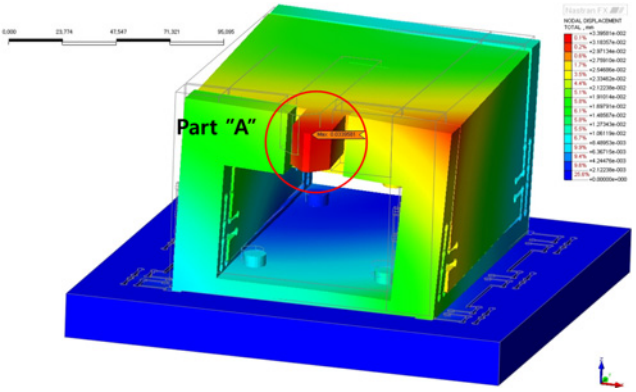

Fig. 6 Deformation of the FEM model for ECTS (cutting load)

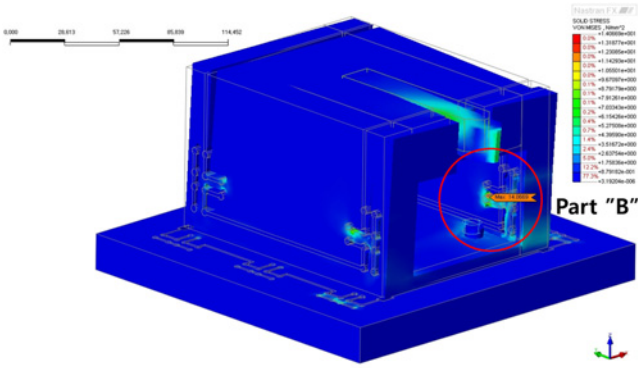

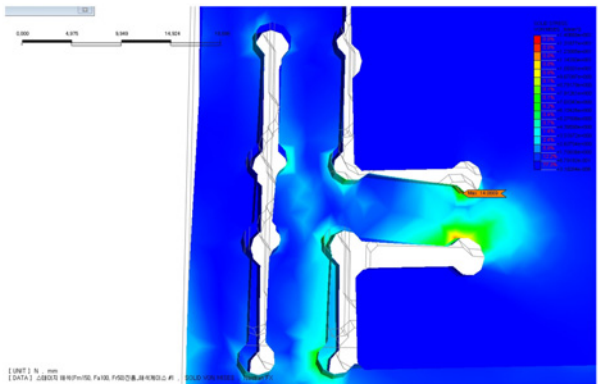

Fig. 7 Von Mises stress distribution of the FEM model for ECTS (cutting load)

applied to the machining tool. Fig. 5 shows the restraint conditions and the machining force, and Table 1 shows the material property of ECTS.

3.2.2 Review of the displacement and safety of the flexure hinge

Finite element analysis was used in this study to minimize the displacement of the stage due to the machining force and to come up with a design by considering the control capability of the stage, thereby identifying any possible crack in the ECTS hinge. The results of the finite element analysis of the deformation and stress distribution of the micro-stage are as follows. Fig. 6 shows the overall deformation of the micro-stage against the maximum machining force, with a 33.95 μm maximum displacement of Part "A".

Table 2 Displacement and stress results

Material	Maximum displacement	Maximum von mises stress	Safety factor
Aluminum	33.95 μm	14.067 N/mm^2	34.3

Table 3 Performance of PSt 150/10/40 VS15 PZT

Maximum stroke (μm)	Generation force	Length L (mm)	Resonance frequency (kHz)
55/40	3,500 N	46	20

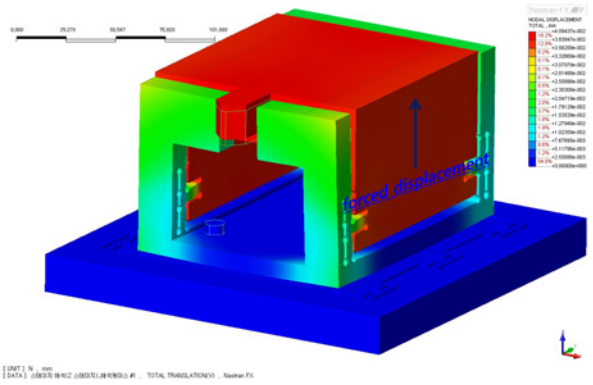

Fig. 8 Deformation of the FEM model for ECTZ (Z direction force displacement)

The distribution of the equivalent stress against the machining force in the micro-stage is shown in Fig. 7 shows the full distribution in Part “B”.

A close review of Fig. 7 shows that the stress is concentrated in Part “C”, with a 14.067 N/mm^2 maximum equivalent stress and a safety index of 34.3. No crack in the hinge structure is expected to be detected. Table 2 shows the resulting maximum equivalent stress.

3.3 Finite element analysis considering the PZT displacement

The Error Compensation Tool Servo is governed mainly by the piezo-electric element by design. The performance of the PSt150/7/40 VS15 PZT actuator, a piezo-electric element manufactured by Piezomechanik, Inc., is shown in Table 3.

3.3.1 Review of the stability of the Z hinge structure

The results of the finite element analysis of the displacement and stress distribution detected in the micro-stage when the 40 μm force displacement generated by the piezo-electric element was applied along the Z axis to the Z stage of ECTS are as follows. Fig. 8 shows the overall deformation of the micro-stage against the maximum displacement of the piezo-electric element, with a 40.94 μm displacement.

The equivalent stress distribution against the Z direction force displacement generated in the micro-stage is shown in Fig. 9 The analysis of the full stress distribution in Part “D” turned up very stable data, with a 47.4877 N/mm^2 maximum equivalent stress and a safety ratio of 10.

3.3.2 Review of the stability of the X-Y hinge structure

Fig. 10 shows the results of the finite element analysis of the displacement and stress distribution detected in the micro-stage when

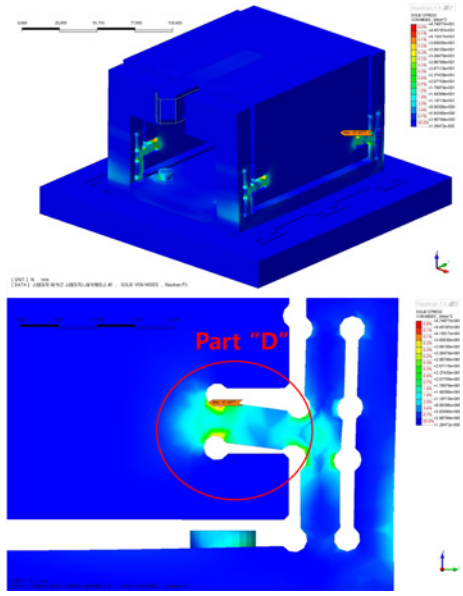

Fig. 9 Von Mises stress distribution of the FEM model for ECTS (Z direction force displacement)

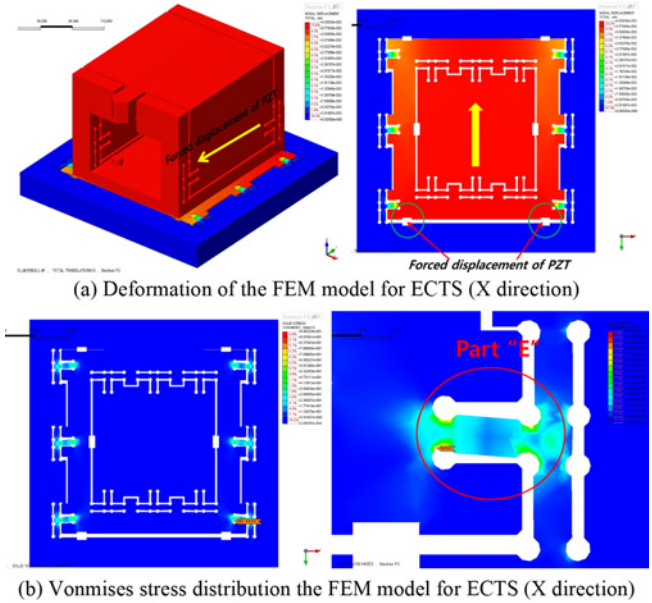

(a) Deformation of the FEM model for ECTS (X direction)

(b) Vonmises stress distribution the FEM model for ECTS (X direction)

Fig. 10 Results of the FEM analysis of ECTS (X direction)

the 40 μm force displacement generated by the piezo-electric element was applied along the X axis direction of the X-Y stage of ECTS, as shown in (b). The maximum displacement of the micro-stage against the maximum displacement of the piezo-electric element was 40.30 μm, and the full stress distribution in Part “E” turned up very stable data, with a 94.622 N/mm^2 maximum equivalent stress and a safety ratio of 5.

Fig. 11 shows the results of the finite element analysis of the displacement and stress distribution detected in the micro-stage when the 40 μm force displacement generated by the piezo-electric element was applied along the Y axis direction of the X-Y stage of ECTS, as

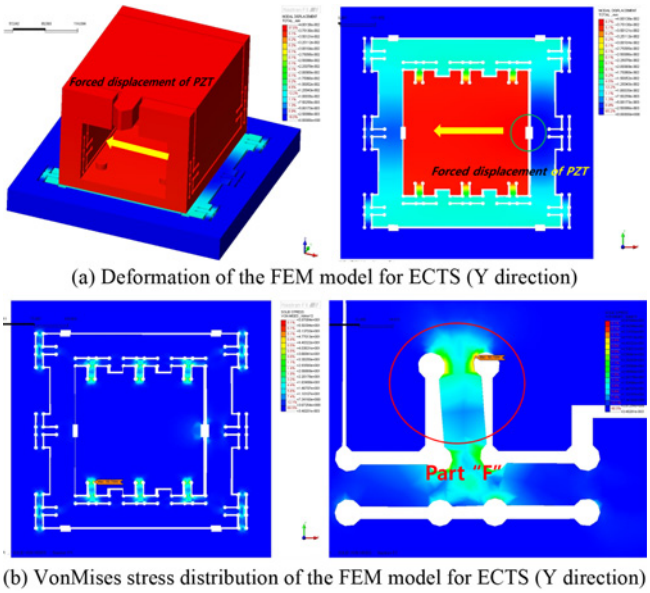

(a) Deformation of the FEM model for ECTS (Y direction)

(b) VonMises stress distribution of the FEM model for ECTS (Y direction)

Fig. 11 Results of the FEM analysis of ECTS (Y direction)

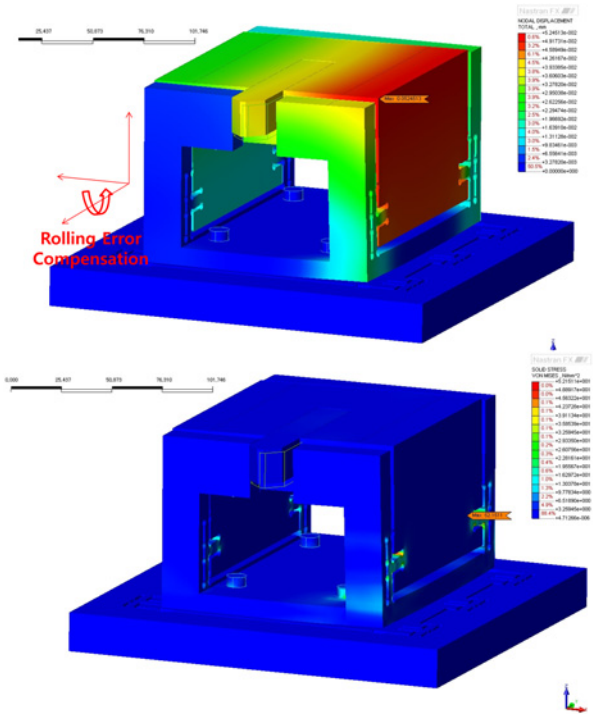

Fig. 12 Results of the FEM analysis of ECTS (rolling motion)

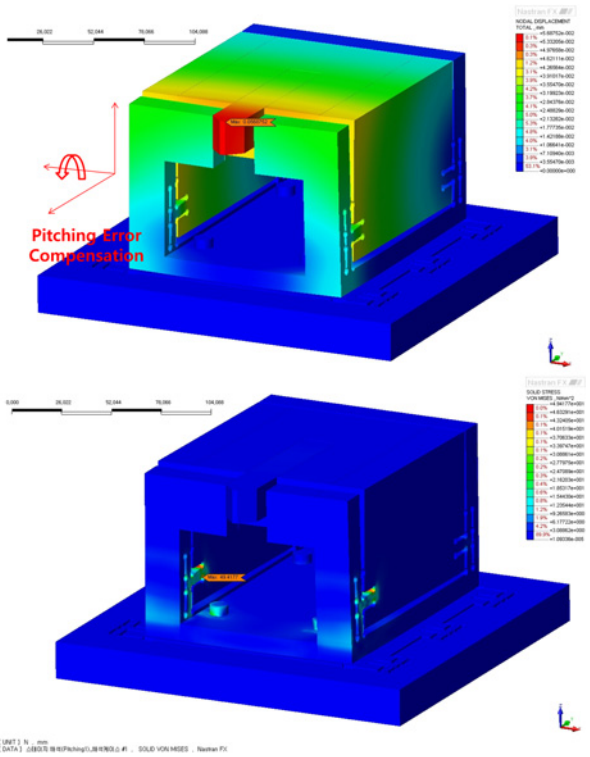

Fig. 13 Results of the FEM analysis of ECTS (pitching motion)

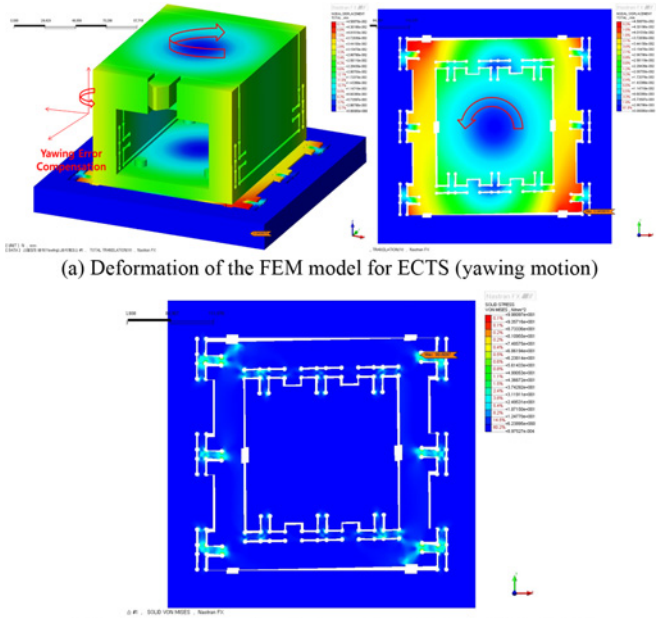

(a) Deformation of the FEM model for ECTS (yawing motion)

(b) Von Mises stress distribution of the FEM model for ECTS (yawing motion)

Fig. 14 Results of the FEM analysis of ECTS (yawing motion)

shown in (b). The hinge along the Y axis direction was designed to be dependent on the X axis stage, with its mutual restraint minimized while supported by the Z hinge structure. The finite element analysis of Part "F" turned up a 40.0138 μm maximum displacement, a 58.7084 N/mm^2 maximum equivalent stress, and a safety ratio of 8.

3.3.3 Review of the rolling, yawing, and pitching error controllability

Most ultra-high-precision machines are designed to analyze and control the linear factor along the X, Y, and Z directions. As this structure is incapable of compensating for irregular errors generated at the nano-level, the Error Compensation Tool Servo of UP3 was developed. It was designed to improve the machining performance by a step higher by compensating for the rolling, yawing, and pitching

Table 4 Displacement and stress results

Force	Maximum displacement (μm)	Maximum von mises stress (N/mm^2)	Safety factor
Machining force	33.95	14.067	34.3
Z axis force displacement	40.94	47.4877	10.16
X-Y hinge structure (X axis direction)	40.30	94.622	5.09
X-Y hinge structure (Y axis direction)	40.01	58.7084	8.22
Rolling error control	52.45	52.1511	9.25
Pitching error control	56.89	49.4177	9.763
Yawing error control	45.88	99.8097	4.83

errors, respectively, that are detected during ultra-high-precision machining. Each of these element values was analyzed through finite element analysis to assess its stability. In Fig. 12, a 40 μm force displacement was applied to the right side of the Z hinge structure to inspect its rolling controllability. The test turned up a 52.45 μm maximum displacement, a 52.1511 N/mm^2 maximum equivalent stress, and a safety ratio of 9.25. Fig. 13 assesses the pitching controllability of the Z hinge structure with a 56.875 μm maximum displacement, a 49.4177 N/mm^2 maximum equivalent stress, and a safety ratio of 9.7. The results of the yawing controllability are shown in Fig. 14, with a 45.88 μm maximum displacement, a 99.8097 N/mm^2 maximum equivalent stress, and a safety ratio of 4.8. The finite element analysis showed a stable result when the piezo-electric element generated a 40 μm maximum displacement, which is an excellent result given the practical range of ±10 μm.

3.4 Results of the finite element analysis

After assessing the validity of the compensation for the rolling, yawing, and pitching errors to compare the accuracy of the results of the analysis of ECTS according to the displacement of the random processing force and the piezo-electric element, its structure was proven capable of generating stable control performance given the maximum displacement of the piezo-electric element, with a safety ratio exceeding 4.83, well within the practical range of ±10 μm.

4. Conclusion

This study was conducted to verify the validity of the micro-stage design using finite element analysis. To accurately compare the results of the analysis of ECTS according to the displacement of the machining force and the piezo-electric element, the validity of the compensation for the rolling, yawing, and pitching errors was verified. The results of this study can be summed up as follows.

i. The initial rigidity of ECTS was designed to maintain its initial value through reverse interpretation of the artificial machining force (Fm: main cutting force, Fr: radial/thrust cutting force, and Fa: feed cutting force). Its rigidity was kept higher than the maximum machining force, as the displacement during the machining, which was observed when the operators concentrated only on the control performance, made it difficult to achieve optimal control performance.

ii. The finite element analysis of the displacement property of the piezo-electric element in the Z hinge structure and the X-Y hinge structure turned up very stable results.

iii. A structure that can respond to rolling, pitching, and yawing errors was designed, and it turned up very stable analysis results.

ACKNOWLEDGEMENT

This work was supported by the Human Resource Training Program for Regional Innovation and Creativity through the Ministry of Education and National Research Foundation of Korea (NRF-2014H1 C1A1066959).

REFERENCES

1. Geyl, R., “Design and Fabrication of a Three-Mirror, Flat-Field Anastigmat for High-Resolution Earth Observation,” Proc. of SPIE, Vol. 2210, pp. 739-746, 1994.
2. Kim, J. Y., Lee, H. N., Kwac, L. K., Han, J. H., Cho, Y. T., and Jun, C. G., Control Performance Evaluation of Ultra Precision Positioning Apparatus,” Proc. of the International Symposium on Mechatronics and Intelligent Mechanical System for 21 Century, ISIM, pp. 252-255, 2000.
3. Shiraishi, M. and Uehara, K., “In-Process Control of Workpiece Dimension in Turning,” Annals of the CIRP, Vol. 28, No. 1, pp. 333-337, 1979.
4. Becker, P., Dorenwendt, K., Ebeling, G., Lauer, R., Lucas, W., et al., “Absolute Measurement of the (220) Lattice Plane Spacing in a Silicon Crystal,” Physical Review Letters, Vol. 46, No. 23, pp. 1540-1543, 1981.
5. Kim, H.-S. and Kim, E.-J., “Feed-Forward Control of Fast Tool Servo for Real-Time Correction of Spindle Error in Diamond Turning of Flat Surfaces,” International Journal of Machine Tools and Manufacture, Vol. 43, No. 12, pp. 1177-1183, 2003.
6. European Commission, Future and Emerging Technologies, http://ec.europa.eu/programmes/horizon2020/en/h2020-section/future-and-emerging-technologies (Accessed 7 SEP 2016)
7. Kohno, T., Okazaki, Y., Ozawa, N., Mitsui, K., and Omoda, M., Inprocess Measurement and a Workpiece-Referred Form Accuracy Control System (WORFAC): Concept of the Method and Preliminary Experiment,” Precision Engineering, Vol.11, No.1, pp. 9-14, 1989.
8. Falter, P. J., “Diamond Turning of Nonrotationally Symmetric Surfaces,” Dissertation Abstracts International, Vol. 51-04, Section: B, pp. 2019, 1990.
9. Patterson, S. R. and Magrab, E. B., “Design and Testing of a Fast Tool Servo for Diamond Turning,” Precision Engineering, Vol. 7, No. 3, pp. 123-128, 1985.
10. Donaldson, R. R. and Patterson, S. R., “Design and Construction of

a Large, Vertical Axis Diamond Turning Machine," Proc. of SPIE, Vol. 0443, pp. 62-67, 1983.

11. Ljubarsky, S. V., Sobolev, V. G., and Shevtsov, S. E., "Optical surface Fabrication on Ultraprecision Machines," Proc. of SPIE, Vol. 1266, pp. 226-236, 1990.
12. Nakazawa, H., "Principles of Precision Engineering," Oxford University Press, pp. 75-82, 140-167, 1994.
13. Smith, S. T. and Chetwynd, D. G., "Foundations of Ultra-Precision Mechanism Design," pp. 95-128, 1992.
14. Keith Bowen, D., "Development in Nanotechnology," Gordon and Breach Science Publishers, pp. 95-129, 1992.
15. Becker, E. B., Carey, G. F., and Oden, J. T., "Finite Elements, an Introduction: Volume I," The University of Texas at Austin, pp. 242-245, 1981.